Fabrication of ZnxCd1−xSe Nanocrystal-Sensitized TiO2 Nanotube Arrays and Their Photoelectrochemical Properties

ARTICLE *in* THE JOURNAL OF PHYSICAL CHEMISTRY C · AUGUST 2012

Impact Factor: 4.77 · DOI: 10.1021/jp3046966

THE JOURNAL OF PHYSICAL CHEMISTRY C

Article

pubs.acs.org/JPCC

Fabrication of $Zn_xCd_{1-x}Se$ Nanocrystal-Sensitized TiO_2 Nanotube Arrays and Their Photoelectrochemical Properties

Qing Kang,[†,‡] Qingyun Cai,*[,†] Shou Zhuo Yao,[†] Craig A. Grimes,[§] and Jinhua Ye*[,‡]

[†]State Key Laboratory of Chemo/Biosensing and Chemometrics, Department of Chemistry, Hunan University, Changsha 410082, P. R. China

[‡]International Center for Materials Nanoarchitectonics (MANA), National Institute for Materials Science (NIMS), 1-2-1 Sengen, Tsukuba, Ibaraki 305-0047, Japan

[§]State Key Laboratory of Materials-Oriented Chemical Engineering, Nanjing University of Technology, Nanjing, Jiangsu 210009, P. R. China

Supporting Information

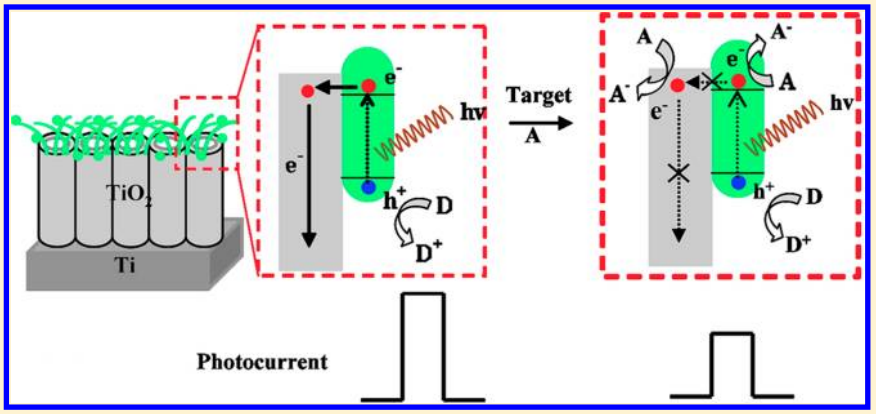

ABSTRACT: $Zn_xCd_{1-x}Se$ $(0 \le x \le 1)$ nanocrystals were pulse electrodeposited onto the surface of anatase TiO_2 nanotube arrays for the first time. The pulse-electrodeposition duty cycle plays a determinative role during the nuclei formation and growth process of the $Zn_xCd_{1-x}Se$ nanocrystals. The composite $Zn_xCd_{1-x}Se/TiO_2$ nanotube arrays exhibit high absorption in the visible light region due to the narrow band gap of $Zn_xCd_{1-x}Se$ and demonstrate a sensitive photoelectrochemical response under visible light illumination with an optimal response achieved for $Zn_{0.8}Cd_{0.2}Se/TiO_2$ electrodes. In photoelectrochemical testing, 9-anthracene carboxylic acid acts as a hole donor resulting in a decrease of the measured photocurrent response. In contrast, 2-anthramine acts as an electron donor, resulting in an increase of the photocurrent response.

1. INTRODUCTION

TiO_2 is a widely used functional material in photocatalytic systems because of its high photocatalytic activity, stability, nontoxicity, oxidative power, and low cost.[1−4] Among all the TiO_2-nanostructured materials studied in recent years, vertically oriented TiO_2 nanotube arrays (NTAs) grown through anodization of titanium have attracted great attention due to their high-surface area structure with vectorial charge transport.[5,6] Such TiO_2 NTAs have been used, for example, as both peroxide and hydrogen sensors.[7,8] The periodic nanoscale−semiconductor interface provides a uniform electric field making it ideally suited for electrochemical modification and surface sensitization with fine crystal structure.[9,10] However, the wide band gap of TiO_2 limits its photoelectrochemical application since it can absorb only UV light ($\lambda < 400$ nm) representing only 3% of the solar-spectrum energy. Modification of TiO_2 with narrow-band gap semiconductors, to enhance the visible light response of the material, is essential for broad implementation of the photoelectrochemical application. To that end, ZnSe and CdSe, our materials of interest here, are active in the visible range and have been successfully used in solar cells.[11,12] Further, ternary semiconductor alloy nanocrystals $(A_xB_{1-x}C)$[13−15] are becoming increasingly important in many areas of nanoscale engineering due to the ability to continuously tune both their physical and optical properties through gradual variation in composition.

In this work ternary $Zn_xCd_{1-x}Se$ $(0 \le x \le 1)$ nanocrystals have been deposited onto the surface of TiO_2 NTAs by pulse electrodeposition. The technological parameters for pulse electrodeposition of $Zn_xCd_{1-x}Se$ nanocrystals were optimized. Anthracene derivatives are chosen to evaluate the photocatalytic capabilities of the hybrid $Zn_xCd_{1-x}Se/TiO_2$ NTAs. The PEC response to anthracene derivatives is strictly due to photocatalysis, with no potential applied. Hybrid $Zn_xCd_{1-x}Se/TiO_2$ NTAs show

Received: May 15, 2012
Revised: July 18, 2012
Published: July 18, 2012

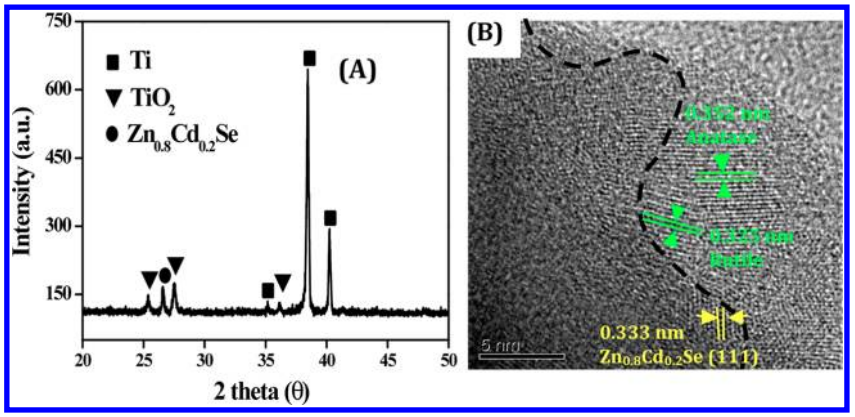

Figure 1. (A) XRD patterns and (B) HRTEM image of $Zn_{0.8}Cd_{0.2}Se/TiO_2$ NTAs.

excellent spectroscopic performance and enhanced photoelectrochemical activities, even to trace amounts of anthracene derivatives.

2. EXPERIMENTAL SECTION

Titanium foil (≥99.8% purity, 0.127 mm thick) was purchased from Aldrich (Milwaukee, WI). NaF, $NaHSO_4$, $CdSO_4$, SeO_2, Na_2S, Na_2SO_4, ethylene glycol (EG), dimethylformamide (DMF), dimethyl sulfoxide (DMSO), 9-anthracene carboxylic acid (9-ACA), 2-anthramine (2-AA), and other reagents of analytical reagent grade were all obtained from commercial sources and used as received. Twice distilled water was used throughout the experiments.

TiO_2 NTAs were prepared by anodization of titanium foil samples.[16] Prior to anodization, the titanium foil samples (1.0 cm × 3.5 cm) were ultrasonically cleaned in acetone for 5 min and then ethanol for 5 min. The cleaned titanium foils were anodized at a constant potential of 15 V in an electrolyte containing 0.1 M NaF and 0.5 M $NaHSO_4$ at room temperature for 3 h in a two-electrode configuration with a platinum cathode. After anodic oxidation, the samples were rinsed with distilled water and dried in air. The resulting amorphous titania NTAs were annealed at 500 °C for 3 h with heating and cooling rates of 2 °C min^{-1} in air to crystallize the tubes and improve their photoactivity.

$Zn_xCd_{1-x}Se$ ($0 \le x \le 1$) nanocrystals were cathodic pulse electrodeposited on the TiO_2 NTA samples. Pulse electrodeposition is a powerful technique to fabricate nanocrystals since its high instantaneous current density can promote the rate of nucleation while reducing the growth rate of the nuclei.[17] The underlying Ti-foil substrate served as an electrical contact, using a conventional three-electrode setup with a Pt-wire counter electrode, and a saturated calomel-electrode (SCE) reference in a bath containing 0.1 M $ZnSO_4$ + $CdSO_4$, 0.1 mM SeO_2, and different electrolyte additives at a pulse "on" potential of −6.0 V and a pulse "off" potential of 0 V. Variable duty cycles (t_{on}/t_{total}) were investigated. Based on previous research,[18−20] an excessive metal/Se ratio was used to ensure successful electrodeposition of $Zn_xCd_{1-x}Se$. Different molar ratios of Zn to Cd precursors were employed, keeping $[Zn^{2+} + Cd^{2+}]/[Se^{2+}]$ at a molar ratio of 1000:1. The loading content was controlled through the deposition duration. The $Zn_xCd_{1-x}Se$ ($0 \le x \le 1$)-modified TiO_2 NTAs were washed several times by distilled water and then heated for 2 h in a N_2 atmosphere.

Sample morphologies were studied using a field-emission scanning electron microscope (FE-SEM, S-4800, Hitachi Instrument). Elemental analyses were carried out on an energy dispersive X-ray spectrometer (EDS) and an energy X-ray mapping spectrometer (EMS). Sample phase was identified by an X-ray diffractometer (XRD, M21X, MAC Science Ltd.) employing Cu Kα radiation (λ = 1.54178 Å). High-resolution transmission electron microscopy (HRTEM) was obtained using a JEM 3010 (JEOL, Tokyo, Japan) operating at 300 kV. UV−vis diffuse reflectance absorption spectra (DRS) were obtained on a UV−vis spectrometer (UV-2500, Shimadzu) and converted from reflection to absorbance by the standard Kubelka−Munk method.

PEC activity was tested using a CHI 660C electrochemical working station (CH Instruments, Austin, TX) in short circuit condition with an electrolyte of 0.6 M Na_2S. The PEC setup is shown in Figure S1 of the Supporting Information. A 300 W Xe lamp (Changtuo Corp., Beijing, China) was used as the solar light source. The light intensity, after passing through a UV-cut filter, was set to 100 mW cm^{-2} as determined by the use of a radiometer (OPHIR, Newport Corp.). No bias potential was applied to the samples during photocatalysis of the anthracene derivatives.

3. RESULTS AND DISCUSSION

3.1. Characterization of Materials. Figure 1A shows the XRD spectrum of the $Zn_{0.8}Cd_{0.2}Se/TiO_2$ NTAs. A characteristic peak at 2θ of 22.61° is assigned to (111) crystal phases of the cubic crystal $Zn_{0.8}Cd_{0.2}Se$ (JCPDS 65-8875). Both anatase (characteristic peak: 25.39°) and rutile (characteristic peaks: 27.57°, 36.11°) phases for TiO_2 NTAs are observed, with a rutile barrier layer underlying the anatase nanotubes.[21] The other peaks are assigned to the Ti substrate. The HRTEM image in Figure 1B depicts the fine structure of the $Zn_{0.8}Cd_{0.2}Se/TiO_2$ NTAs. The fringe spacing of 0.333 nm is indexed to the (111) plane of the zinc cadmium selenide. The fringe spacings of 0.352 and 0.325 nm correspond to the (101) and (110) planes of anatase and rutile TiO_2, respectively. These results indicate that the material prepared by pulse electrodeposition is highly crystalline in nature, is essential for a good photocatalytic material, and may impact the local titania nanostructure.

The architecture of the $Zn_{0.8}Cd_{0.2}Se/TiO_2$ NTAs surface was characterized by element X-ray mapping. Figure 2 (b−f) shows the elemental distribution of Ti, O, Zn, Cd, and Se, respectively. The images suggest that $Zn_{0.8}Cd_{0.2}Se$ is compact and well-attached to the TiO_2 NTAs surface. EDX analysis, Figure 3, shows the presence of Zn, Cd, and Se in both grasslike and

dx.doi.org/10.1021/jp3046966 | J. Phys. Chem. C 2012, 116, 16885−16892

spherical nanocrystals. The elemental composition reveals that the atomic ratio of (Zn + Cd)/Se is not 1:1, presumably due to the low pH value of the plating solution as noted by Peng and co-workers.[22] Furthermore, the ratio of Zn to Cd incorporated in nanocrystals is in contradiction with the molar ratio of Zn^{2+} to Cd^{2+} in solution; more Cd was deposited due to the higher reactivity of Cd^{2+} with respect to Zn^{2+}.[23] Similar results are reported by Natarajan,[18] Bouroushian,[19] and Murali and co-workers.[20] The material characterizations indicate uniform fabrication, over large sample areas, of the $Zn_{0.8}Cd_{0.2}Se/TiO_2$ NTA heterojunction photocatalyst.

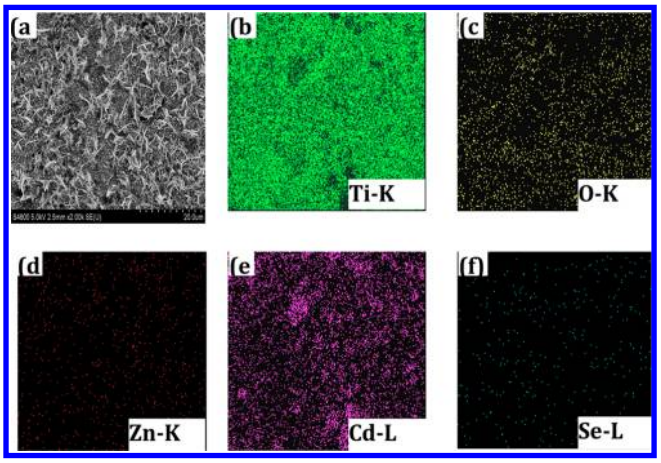

Figure 2. EMS analyses of $Zn_{0.8}Cd_{0.2}Se/TiO_2$ NTAs. (a) Whole top view of the nanotubes and (b–f) EMS of Ti–K, O–K, Zn–K, Cd–L, and Se–L, respectively.

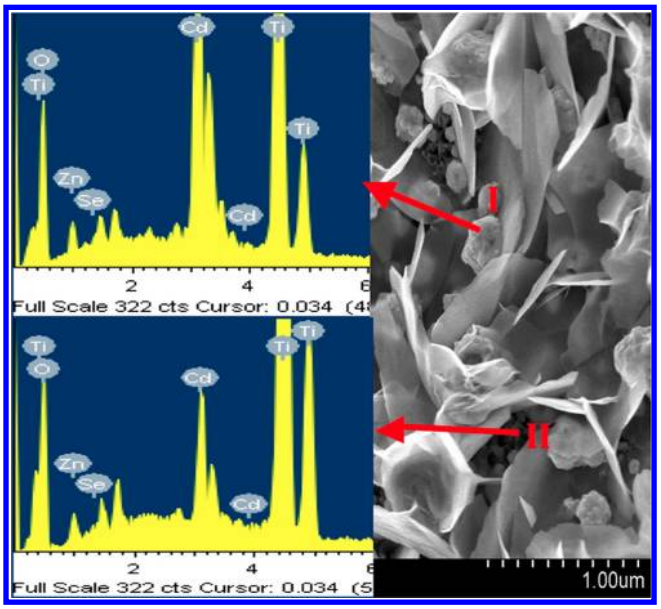

Figure 3. EDX analyses of $Zn_{0.8}Cd_{0.2}Se/TiO_2$ NTAs at two different sites.

3.2. Photoelectrochemical Properties. Photoelectrochemical quantification of high sensitivity requires high-photoelectrical activity. The photoelectrical activity of the $Zn_xCd_{1-x}Se/TiO_2$ NTA electrode is dependent upon the composition and crystal structure of the $Zn_xCd_{1-x}Se$ nanocrystals that, in turn, are dependent upon electrodeposition variables, including plating solution, duty cycles, and temperature.

As shown in Figure 4A, the unmodified-TiO_2 NTAs show a minimal photoelectrical response, while the $Zn_xCd_{1-x}Se/TiO_2$ NTAs show dramatically higher photocurrents due to the improved harvesting of visible light. The photocurrent depends on the nanocrystal composition, with the highest photoactivity observed with the $Zn_{0.8}Cd_{0.2}Se/TiO_2$ NTAs.

The short circuit current desnity (J_{sc}) of the $Zn_{0.8}Cd_{0.2}Se/TiO_2$ NTAs is significantly greater than that of the ZnSe- or CdSe-deposited TiO_2 NTAs, with J_{sc} versus nanocrystal compositions shown in Figure 4B. Specific J_{sc} values per composition are 0.564 mA/cm^2 for $Zn_{0.2}Cd_{0.8}Se$, 0.718 mA/cm^2 for $Zn_{0.8}Cd_{0.2}Se$, 0.459 mA/cm^2 for CdSe, and 0.124 mA/cm^2 for ZnSe. The presence of two maxima in the photoelectrocatalytic performance of $Zn_xCd_{1-x}Se/TiO_2$ is similar to the observation on (CdS-ZnS)/TiO_2 reported by Antoniadou et al.[24] J_{sc} values were very modest in the cases of $Zn_{0.4}Cd_{0.6}Se$ and $Zn_{0.6}Cd_{0.4}Se$. Murali and co-workers[20] also reported that large amounts of heterogeneous elements could distort the semiconductor lattice, thus, hindering charge transport in the nanocrystals.

The optical properties of the $Zn_xCd_{1-x}Se/TiO_2$ NTAs within 200–850 nm were further investigated by measuring the UV–vis DRS. As shown in Figure 5A, absorbance intensity increases as the Zn composition increases, while the overall behavior remains similar. Energy band gaps (E_g) for the $Zn_xCd_{1-x}Se/TiO_2$ NTAs, calculated from the observed UV–vis DRS peaks, are shown in Figure 5B as a function of composition (x). Variation of the energy band gaps with composition is linear: the band gap increases from 2.16 eV for ZnSe/TiO_2 NTA to 1.98 eV for

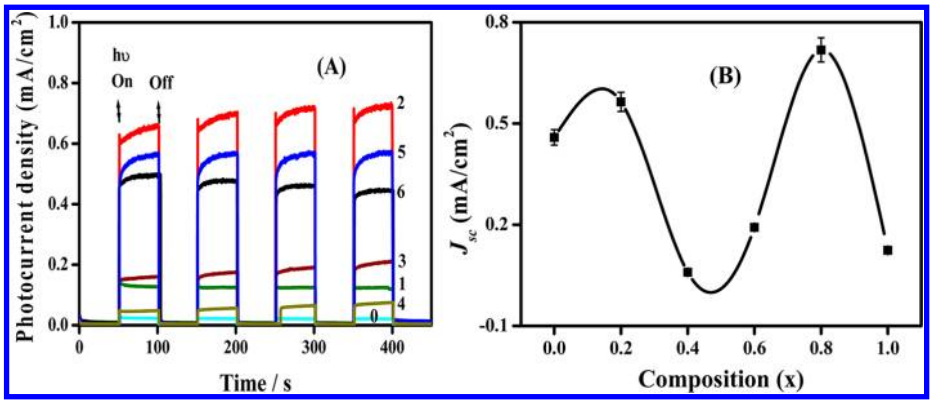

Figure 4. (A) Photocurrent response of pure-TiO_2 NTAs (curve 0) and $Zn_xCd_{1-x}Se/TiO_2$ NTAs at compositions of x = 1, 0.8, 0.6, 0.4, 0.2, and 0 for curves 1–6, respectively. (B) Effect of composition x on short circuit photocurrent density for $Zn_xCd_{1-x}Se/TiO_2$ NTAs.

dx.doi.org/10.1021/jp3046966 | J. Phys. Chem. C 2012, 116, 16885–16892

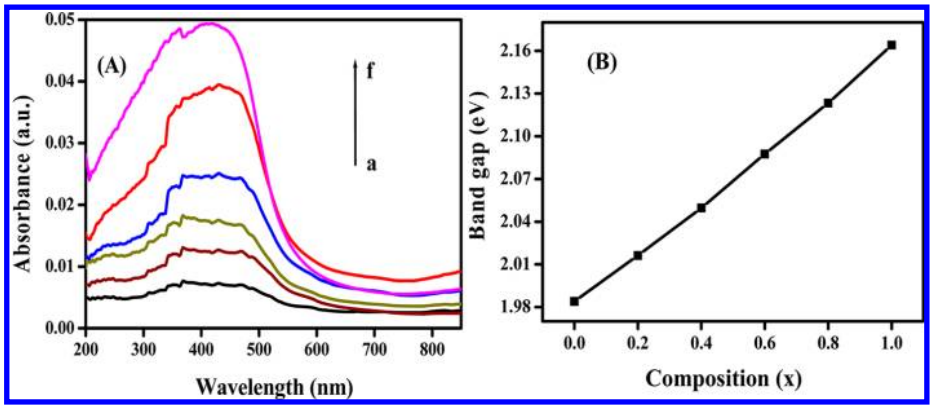

Figure 5. (A) UV−vis DRS of $Zn_xCd_{1-x}Se/TiO_2$ NTAs at compositions of $x = 0$, 0.2, 0.4, 0.6, 0.8, and 1 for curves a−f, respectively. (B) Variations of the band gap energy of $Zn_xCd_{1-x}Se/TiO_2$ NTAs vs the composition coefficient (x).

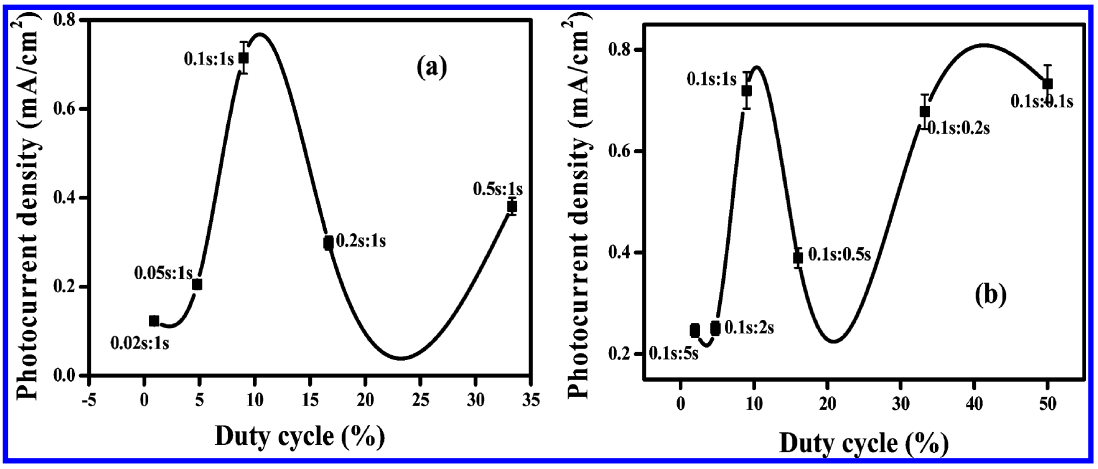

Figure 6. Effect of duty cycle on the photocurrent response of $Zn_{0.8}Cd_{0.2}Se/TiO_2$ NTAs: (a) t_{off} kept the same and (b) t_{on} kept the same.

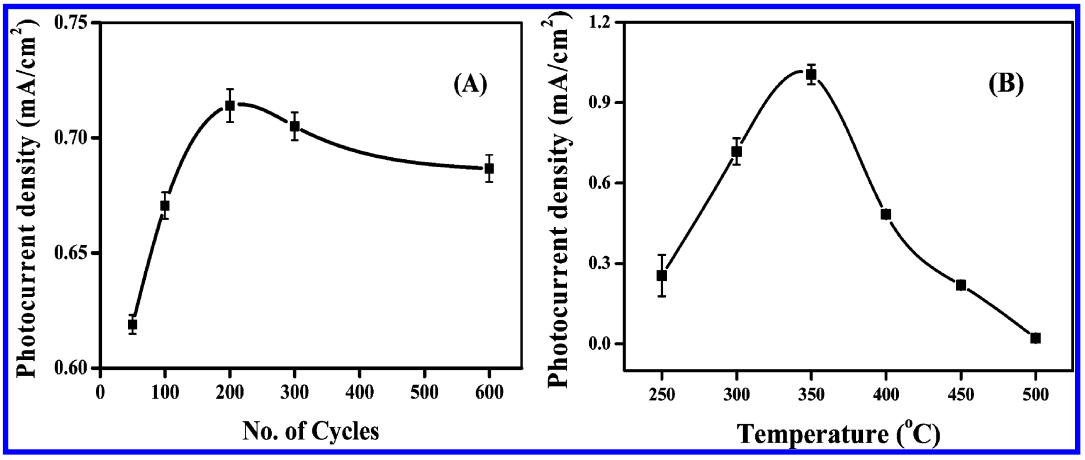

Figure 7. (A) Effect of deposition cycles and (B) heat treatment temperature on the photocurrent response of $Zn_{0.8}Cd_{0.2}Se/TiO_2$ NTAs.

$CdSe/TiO_2$ NTA. This result indicates that ZnSe and CdSe have excellent miscibility.

In the pulse-electrodeposition protocol, the pulse potential is to provide high nucleation density, and the short pulse duration is to terminate the three-dimensional growth of nanocrystals after the nucleation step. A sufficiently long rest duration must be used so that the concentration of electrolyte can be restabilized at the electrode−solution interface by mass-transport diffusion. Figure 6a shows the effect of the electrodeposition duty cycle on the photocurrent response of $Zn_{0.8}Cd_{0.2}Se/TiO_2$ NTA films where t_{off} was fixed at 1 s, and t_{on} was varied across 0.02, 0.05, 0.1, 0.2, and 0.5 s, corresponding to duty cycles of approximately 2, 4.8, 9.1, 16.7, and 33.3%, respectively. The highest photocurrent is achieved with a 9.1% duty-cycle deposition. Increasing the duty cycle over 9.1% leads to the formation of a $Zn_{0.8}Cd_{0.2}Se$ layer covering the pores of the TiO_2 NTA surface that, in turn, reduces the surface area and, hence, the photocurrent. The data of Figure 6b complement that of Figure 6a, but in this case t_{on} is kept constant at 0.1 s with t_{off} varied.

dx.doi.org/10.1021/jp3046966 | J. Phys. Chem. C 2012, 116, 16885−16892

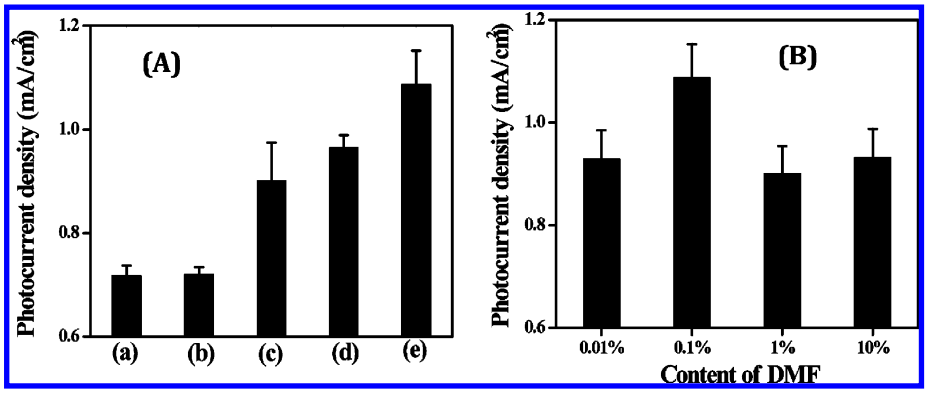

Figure 8. (A) Photocurrent response of $Zn_{0.8}Cd_{0.2}Se/TiO_2$ NTAs prepared by pulse electrodeposition (a) without or (b–e) with different supporting electrolytes: (b) Na_2SO_4, (c) EG, (d) DMSO, and (e) DMF. (B) Photocurrent response of $Zn_{0.8}Cd_{0.2}Se/TiO_2$ NTAs prepared by pulse electrodeposition in 0.01, 0.1, 1, and 10% DMF solution.

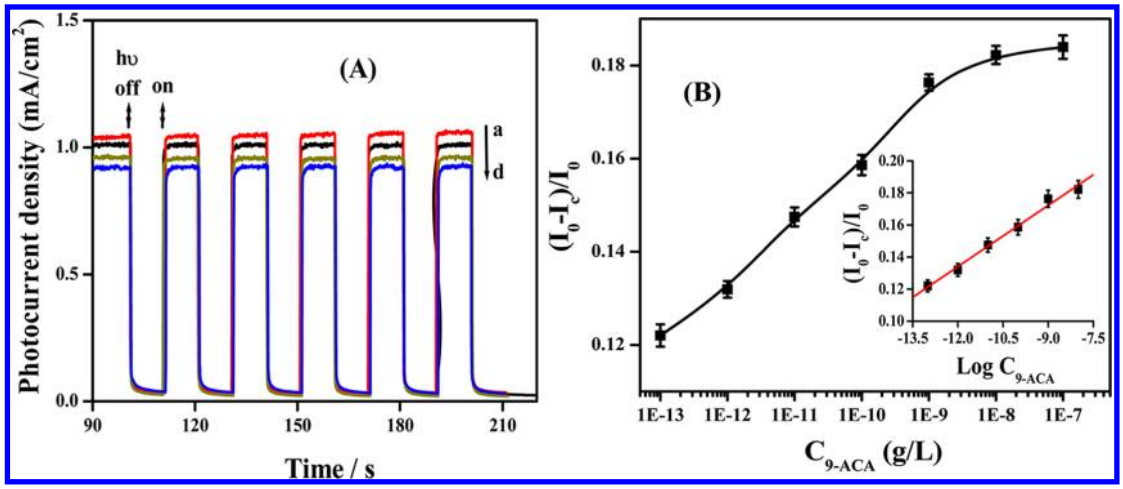

Figure 9. (A) Photocurrent response of $Zn_{0.8}Cd_{0.2}Se/TiO_2$ NTAs in 0.6 M Na_2S containing different concentrations of 9-ACA: (a) 0 g/L, (b) 1 fg/L, (c) 10 pg/L, and (d) 0.1 μg/L. (B) Calibration curves for the photochemical assay for 9-ACA determination.

The loading mass of the $Zn_{0.8}Cd_{0.2}Se$ nanocrystals is dependent on both the duty cycle and the number of deposition cycles. Figure 7A shows that photocurrent increases with the number of deposition cycles up to 200, beyond which it slowly decreases. A postdeposition annealing step is used to improve crystallinity. Figure 7B shows the photocurrent response of $Zn_{0.8}Cd_{0.2}Se/TiO_2$ NTA films as a function of postdeposition annealing temperature. Annealing temperatures above 350 °C result in the nanocrystals sintering together to form a low-surface area compact film with a corresponding decrease in measured photocurrent. Earlier studies[25] indicate that electronic transmission in small grains is more efficient than in large crystals; recombination of photogenerated charges is suppressed in small grains due to steric hindrance, resulting in larger photocurrents.

Previous reports[26−28] indicate that the addition of organic additives to the electrodeposition bath can be used to reduce the nanocrystal surface energy. Figure 8A compares the short circuit photocurrent density of $Zn_{0.8}Cd_{0.2}Se/TiO_2$ NTAs prepared by pulse electrodeposition (a) without additional additive and with (b) Na_2SO_4, (c) EG, (d) DMSO, and (e) DMF. $Zn_{0.8}Cd_{0.2}Se/TiO_2$ NTAs obtained in conductive organic electrolytes show enhanced PEC performance, with those prepared in DMF showing the highest photocurrent. Figure 8B shows the effect of DMF concentration with maximum performance found with 0.1 vol % DMF. Higher organic electrolyte concentrations result in higher viscosity films, which in turn prevent nuclei formation; hence, fewer crystals are deposited onto the substrate.[26−28]

3.3. Photoelectrochemical Response to Anthracene Derivatives. Figure 9A shows the photocurrent response of $Zn_{0.8}Cd_{0.2}Se/TiO_2$ NTA samples in 0.6 M Na_2S containing different concentrations of the anthracene derivative 9-ACA. The photocurrent response is fully reproducible with no decrease through repeated illumination–dark cycles. The photocurrent response decreases with increasing 9-ACA concentration, spanning 8 orders of magnitude, 1 fg/L to 0.1 μg/L. The decrease in photocurrent is logarithmically proportional to 9-ACA concentrations in the range of 0.1 pg/L to 10 ng/L, as shown in the inset of Figure 9B.

In contrast to 9-ACA, anthracene derivative 2-AA behaved as an electron donor, increasing the photocurrent magnitude (see Figure 10A). The change in photocurrent amplitude is linearly proportional to the logarithm of 2-AA concentrations in the range of 1 pg/L to 0.1 μg/L as shown in Figure 10B, with a correlation coefficient of 0.999. The increase in photocurrent with the 2-AA concentration in solution indicates that the TiO_2 NTA surface had not yet been saturated by 2-AA in the investigated concentration range. The reaction order (n) can be determined according to the following equation:

$$\log I_c = \log k + n \log C_{2\text{-AA}}$$

where k is the reaction rate constant (s^{-1}). Both the $Zn_{0.8}Cd_{0.2}Se/TiO_2$ and pure-TiO_2 NTA electrodes present a

dx.doi.org/10.1021/jp3046966 | J. Phys. Chem. C 2012, 116, 16885−16892

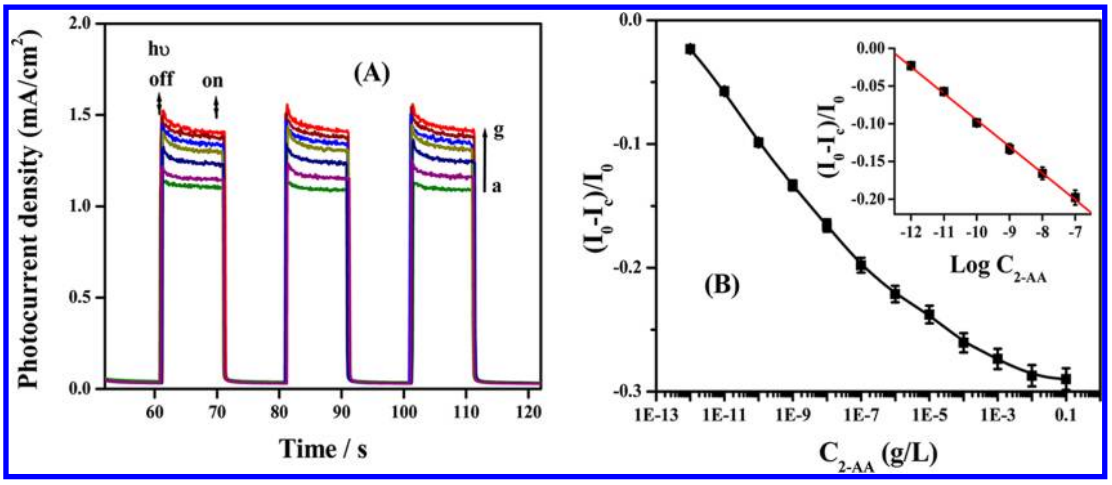

Figure 10. (A) Photocurrent response of $Zn_{0.8}Cd_{0.2}Se/TiO_2$ NTAs in 0.6 M Na_2S containing different concentrations of 2-AA: (a) 0 g/L, (b) 10 pg/L, (c) 1 ng/L, (d) 0.1 μg/L, (e) 10 μg/L, (f) 1 mg/L, and (g) 0.1 g/L. (B) Calibration curves for the photochemical assay for 2-AA determination.

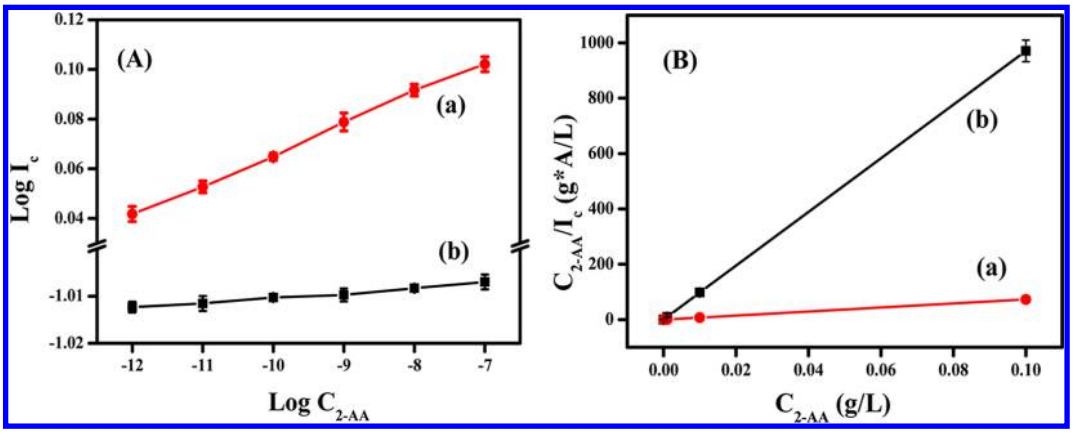

Figure 11. (A) Plot of log photocurrent vs log concentration of 2-AA for (a) $Zn_{0.8}Cd_{0.2}Se/TiO_2$ NTAs and (b) pure-TiO_2 NTAs. (B) Analyses of the photocurrents and 2-AA concentration for (a) $Zn_{0.8}Cd_{0.2}Se/TiO_2$ NTAs and (b) pure-TiO_2 NTAs using the Langmuir equation.

reaction order close to one with rate constants of 1.5 ± 0.04 s^{-1} for $Zn_{0.8}Cd_{0.2}Se/TiO_2$ NTA and 0.1 ± 0.002 s^{-1} for the pure-TiO_2 NTA, representing a 15× increase in electron transfer efficiency due to the presence of $Zn_{0.8}Cd_{0.2}Se$ nanocrystals.

Investigations into the adsorption phenomenon can be performed based on the 2-AA concentration-dependent variation of the photocurrent. It is reasonable to suppose that there are no lateral interactions between the adsorbed species. Thus, the adsorption equilibrium constant (b) can be determined by the Langmuir equation:[29]

$$\theta = \frac{bC_{2\text{-AA}}}{1 + bC_{2\text{-AA}}}$$

If $\theta = \Gamma/\Gamma_{max}$ (where Γ represents the surface 2-AA concentration and Γ_{max} the surface 2-AA concentration at saturation), then

$$\frac{C_{2\text{-AA}}}{\Gamma} = \frac{1}{b\Gamma_{max}} + \frac{C_{2\text{-AA}}}{\Gamma_{max}}$$

Considering that the photocurrent is proportional to the surface concentration of 2-AA, the above equation can be written as

$$\frac{C_{2\text{-AA}}}{I_c} = \frac{1}{bI_{max}} + \frac{C_{2\text{-AA}}}{I_{max}}$$

When $C_{2\text{-AA}}/I_c$ is plotted as a function of $C_{2\text{-AA}}$ for the $Zn_{0.8}Cd_{0.2}Se/TiO_2$ and pure-TiO_2 NTA electrodes (Figure 11B), good linearity was found with a correlation coefficient close to 0.99, confirming that this adsorption phenomenon is related to a Langmuir isotherm. From the intercept and slope, adsorption equilibrium constants are calculated to be 10.1 ± 0.02 for the $Zn_{0.8}Cd_{0.2}Se/TiO_2$ electrode and 9.01 ± 0.01 for the pure-TiO_2 NTA electrode. This result indicates that 2-AA adsorption occurs more readily on the $Zn_{0.8}Cd_{0.2}Se/TiO_2$ NTA electrode than on the pure-TiO_2 NTA electrode, further confirming that the nanocrystals are more effective in adsorbing and subsequently oxidizing 2-AA.

The reproducibility of the $Zn_{0.8}Cd_{0.2}Se/TiO_2$ NTA electrodes was evaluated by determining the intra-assay and interassay relative standard deviation (RSD). Using a $Zn_{0.8}Cd_{0.2}Se/TiO_2$ NTA electrode for analysis of a 0.1 mg/L 2-AA solution, across six measurements an intra-assay RSD of 4.24% was found. The interassay RSD across five different $Zn_{0.8}Cd_{0.2}Se/TiO_2$ NTA electrodes was found to be 5.19%. The results indicate good reproducibility of the fabrication protocol.

Figure 12 is an illustrative diagram depicting transport of the photogenerated electrons and holes in the $Zn_{0.8}Cd_{0.2}Se/TiO_2$ NTA electrodes. The presence of electron quenchers and donors results in a corresponding decrease and increase, respectively, of the photocurrent.

dx.doi.org/10.1021/jp3046966 | J. Phys. Chem. C 2012, 116, 16885−16892

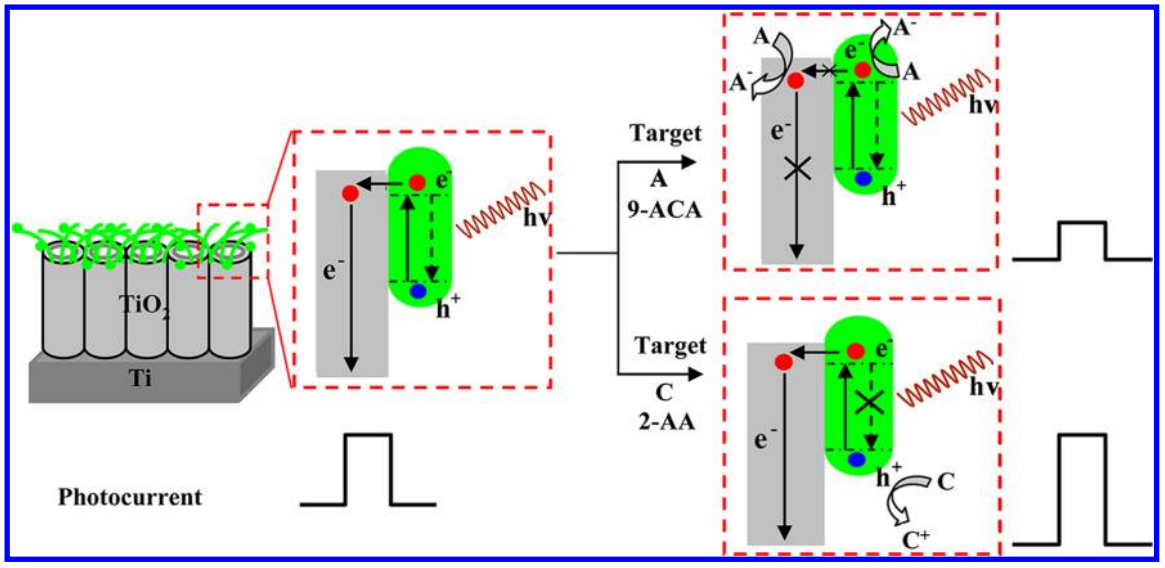

Figure 12. Transport of the photogenerated electrons and holes in $Zn_{0.8}Cd_{0.2}Se/TiO_2$ NTA electrodes.

4. CONCLUSIONS

Hybrid $Zn_xCd_{1-x}Se/TiO_2$ nanotube-array photoelectrodes are fabricated by pulse electrodeposition of $Zn_xCd_{1-x}Se$ on TiO_2 NTA films. The effects of the $Zn_xCd_{1-x}Se$ plating solution and deposition duty cycles on the photoelectrical response of the resulting samples are detailed. Modification of TiO_2 NTA films with $Zn_xCd_{1-x}Se$ nanocrystals significantly improves the electron-transfer efficiency. The presence of electron quenchers and donors results in a corresponding decrease and increase, respectively, of the photocurrent. With the benefit of the creation of highly reactive sites on the modified $Zn_{0.8}Cd_{0.2}Se$ nanocrystals, a remarkable increase of the anthracene-derivative phtotoelectrocatalytical reaction rate at the $Zn_{0.8}Cd_{0.2}Se/TiO_2$ electrode was observed. We believe this study opens a new perspective for the application of semiconductors in the analytical detection field.

■ ASSOCIATED CONTENT

Supporting Information

Configuration of the photoelectrochemical cell (Figure S1) and FESEM images of the $Zn_{0.8}Cd_{0.2}Se/TiO_2$ NTA samples (Figure S2). This material is available free of charge via the Internet at http://pubs.acs.org.

■ AUTHOR INFORMATION

Corresponding Author

*Q.C.: e-mail, qycai0001@hnu.cn. J.Y.: e-mail, Jinhua.YE@nims.go.jp.

Notes

The authors declare no competing financial interest.

■ ACKNOWLEDGMENTS

This work was supported by the National Basic Research Program of China under Grant 2009CB421601; the National Science Foundation of China (Grants 21175038 and 51008149); the World Premier International Research Center Initiative on Materials Nanoarchitectonics, MEXT; the Global COE Program of the Tokyo Institute of Technology; and the Japan Science and Technology Agency (JST) Precursory Research for Embryonic Science and Technology (PRESTO) Program.

■ REFERENCES

(1) Teramura, K.; Maeda, K.; Saito, T.; Takata, T.; Saito, N.; Inoue, Y.; Domen, K. *J. Phys. Chem. B* **2006**, *110*, 4500−4501.
(2) Wilson, J. N.; Idriss, H. *J. Am. Chem. Soc.* **2002**, *124*, 11284−11285.
(3) Li, X.; Liu, H.; Yue, P.; Sun, Y. *Environ. Sci. Technol.* **2000**, *34*, 4401−4406.
(4) Li, X.; Liu, H. *Environ. Sci. Technol.* **2005**, *39*, 4614−4620.
(5) Grimes, C.; Mor, G. K. *TiO_2 Nanotube Arrays: Synthesis, Properties, and Applications*; Springer: Norwell, MA, 2009.
(6) Grimes, C. A.; Varghese, O. K.; Ranjan, S. *Light, Water, Hydrogen: The Solar Generation of Hydrogen by Water Photoelectrolysis*; Springer: Norwell, MA, 2008.
(7) Varghese, O. K.; Gong, D.; Paulose, M.; Ong, K. G.; Grimes, C. A. *Sens. Actuators, B* **2003**, *93*, 338−344.
(8) Chen, D.; Zhang, H.; Li, X.; Li, J. *Anal. Chem.* **2010**, *82*, 2253−2261.
(9) Yang, L.; Luo, S.; Liu, R.; Cai, Q.; Xiao, Y.; Liu, S.; Su, F.; Wen, L. *J. Phys. Chem. C* **2010**, *114*, 4783−4789.
(10) Zhang, H.; Quan, X.; Chen, S.; Yu, H.; Ma, N. *Chem. Mater.* **2009**, *21*, 3090−3095.
(11) Wang, K.; Chen, J.; Zhou, W.; Zhang, Y.; Yan, Y.; Pern, J.; Mascarenhas, A. *Adv. Mater.* **2008**, *20*, 3248−3253.
(12) Lee, Y. L.; Huang, B. M.; Chien, H. T. *Chem. Mater.* **2008**, *20*, 6903−6905.
(13) Mourad, D.; Czycholl, G. *Eur. Phys. J. B* **2010**, *78*, 497−507.
(14) Ng, S.; Hassan, Z.; Abu Hassan, H. *Appl. Phys. Lett.* **2007**, *91*, 081909−081903.
(15) Mostefai, N.; Bouarissa, N.; Belkhir, A. *Adv. Mater. Res. (Berlin, Ger.)* **2011**, *324*, 249−252.
(16) Kang, Q.; Lu, Q.; Liu, S.; Yang, L.; Wen, L.; Luo, S.; Cai, Q. *Biomaterials* **2010**, *31*, 3317−3326.
(17) Frari, D. D.; Diliberto, S.; Stein, N.; Boulanger, C.; Lecuire, J. M. *J. Appl. Electrochem.* **2006**, *36*, 449−454.
(18) Natarajan, C.; Nogami, G.; Sharon, M. *Thin Solid Films* **1995**, *261*, 44−51.
(19) Bouroushian, M.; Kosanovic, T. J. *Solid State Electrochem.* **2006**, *10*, 223−229.
(20) Murali, K.; Balasubramanian, M. *Current Applied Physics* **2010**, *10*, 734−739.
(21) Varghese, O. K.; Gong, D.; Paulose, M.; Grimes, C. A.; Dickey, E. C. *J. Mater. Res.* **2003**, *18*, 156−165.
(22) Peng, X.; Zhang, J.; Wang, X.; Wang, Y.; Zhao, L.; Meng, G.; Zhang, L. *Chem. Phys. Lett.* **2001**, *343*, 470−474.
(23) Ge, J.; Xu, S.; Zhuang, J.; Wang, X.; Peng, Q.; Li, Y. *Inorg. Chem.* **2006**, *45*, 4922−4927.

(24) Antoniadou, M.; Daskalaki, V. M.; Balis, N.; Kondarides, D. I.; Kordulis, C.; Lianos, P. *Appl. Catal., B* **2011**, *107*, 188−196.
(25) Baker, D. R.; Kamat, P. V. *Adv. Funct. Mater.* **2009**, *19*, 805−811.
(26) Bunge, S. D.; Krueger, K. M.; Boyle, T. J.; Rodriguez, M. A.; Headley, T. J.; Colvin, V. L. *J. Mater. Chem.* **2003**, *13*, 1705−1709.
(27) Kazes, M.; Lewis, D. Y.; Banin, U. *Adv. Funct. Mater.* **2004**, *14*, 957−962.
(28) Manna, L.; Scher, E. C.; Li, L.; Alivisatos, A. P. *J. Am. Chem. Soc.* **2002**, *124*, 7136−7145.
(29) Ju, H.; Leech, D. *J. Electroanal. Chem.* **2000**, *484*, 150−156.